

Fachbereich 13  
Institut für Theoretische Physik  
Goethe-Universität Frankfurt am Main

# **The Gravo-thermal Fluid Model of Self-Interacting Dark Matter Halos with a Central Mass**

**Abschlussarbeit zur Erlangung des akademischen Grades  
Bachelor of Science in Physik**

vorgelegt von Lukas Kerim Arda, geb. am 30.05.2000 in  
Frankfurt am Main

Erstgutachterin: Prof.in Dr. Laura Sagunski  
Zweitgutachter: Prof. Dr. Jürgen Schaffner-Bielich

Eingereicht am 19.05.2022

# Contents

<b>1</b>	<b>Abstract</b>	<b>3</b>
<b>2</b>	<b>Introduction</b>	<b>4</b>
2.1	The Lambda-CDM-Model . . . . .	4
2.2	Dark Matter Density Profiles and SIDM Halos . . . . .	6
2.3	Dark Matter Density Spike . . . . .	10
2.4	Aim and Structure of this Thesis . . . . .	12
<b>3</b>	<b>Theoretical Foundations</b>	<b>13</b>
3.1	The Gravo-thermal Fluid Model . . . . .	13
3.2	Thermal Conductivity . . . . .	16
3.3	Central Black Hole Modification . . . . .	18
3.4	Lagrangian Zones . . . . .	20
<b>4</b>	<b>Numerical Approach</b>	<b>22</b>
4.1	Dimensionless equations and quantities . . . . .	22
4.2	Discretization and Initial Data . . . . .	23
4.3	Time Evolution . . . . .	25
<b>5</b>	<b>Results</b>	<b>32</b>
5.1	Adiabatic Black Hole Growth . . . . .	32
5.2	Initial Dark Matter Density Spike . . . . .	33
<b>6</b>	<b>Conclusions</b>	<b>36</b>
6.1	Summary . . . . .	36
6.2	Outlook . . . . .	37
<b>7</b>	<b>Acknowledgement</b>	<b>43</b>
<b>8</b>	<b>Eigenständigkeitserklärung</b>	<b>43</b>

# 1 Abstract

Dark matter is one of the great mysteries in modern-day cosmology. Its properties of it can be studied through observations of gravitational waves emitted by massive object inspirals inside of a dark matter background. This thesis focuses on simulating those dark matter structures, which we call dark matter halos, for the model of self-interacting dark matter. In particular, we are extending the gravothermal fluid model that includes the interaction of the particles as well as gravitational processes by adding a central black hole. These systems containing a black hole surrounded by dark matter are of particular interest since the central black hole over-concentrates dark matter in the inner regions of the halo. During inspirals, this over-density is expected to leave an imprint on the emitted signal.

For our simulation, we use a numerical implementation of the gravothermal fluid model and extend it by inserting the black hole mass and adjusting the fluid equations to account for the additional gravitational pull. With this numerical approach to the system, we can reproduce semi-analytical predictions of the over-densities. We can also show that growth processes are necessary to generate these over-densities, which has implications for the genesis of such systems. The agreement between our simulation and the prediction provides a strong implication that the extended model and its implementation allow us to realistically simulate large structures of dark matter.

## 2 Introduction

Cosmologists seek to describe and understand the nature of the universe. There was already a lot of work invested in this, but we are still facing several unresolved mysteries. The task of finding a cosmological model which describes the structure and dynamics as well as the origin, evolution, and ultimate fate of our universe as we see it is still unfulfilled. Though this may seem maddening to some, it is truly what motivates us and drives our curiosity. Everything not understood tells us, that there is still a lot to explore!

### 2.1 The Lambda-CDM-Model

In modern cosmology there is a popularly accepted model. The Lambda cold dark matter ( $\Lambda$ -CDM) model. This model gives a simple parametrization for the evolution of a universe originating from a Big Bang. It assumes general relativity as the correct theory of gravity on large scales and that the universe is flat. It is often referred to as the standard model of cosmology because it describes key properties of our universe like the cosmic microwave background, the large-scale structure and the accelerated expansion of the universe. The  $\Lambda$ -CDM model assumes that the late time evolution of the universe is driven by three major components. Dark energy (denoted by the  $\Lambda$ ), dark matter and baryonic matter. Baryonic matter is the ordinary form of matter, everything we know is made of and is well studied. The other two components are more of a mystery to cosmologists. Even though they are not well understood, they play a huge role in the  $\Lambda$ -CDM model. Fig. 1 shows the shares of dark energy and dark matter of the total energy density of our universe at the current moment. With the current data, we assume that dark energy and dark matter make up  $\approx 95\%$  of the universe's total energy and dark matter accounts for  $\approx 85\%$  of the universe's matter. While dark energy is used to explain the accelerated expansion of the universe, dark matter is postulated to account for observed gravitational effects that can not be explained solely by ordinary matter, such as galaxy rotation curves, the large-scale structure, etc. (see e.g. [33]).

This thesis is devoted to investigating the nature of dark matter. There are

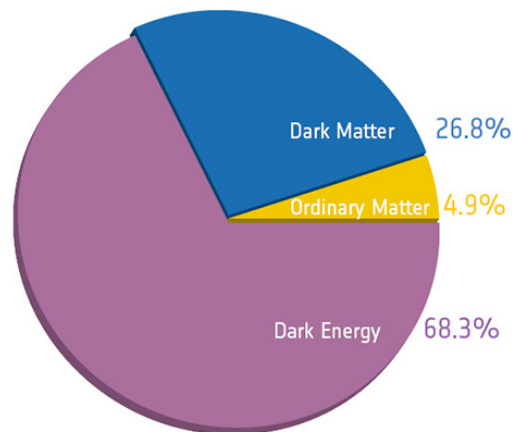


Figure 1: Contributions of the three dominant components of our universe to the total energy density (Reprinted from: [18])

multiple hints for its existence. One striking example is the so-called 'missing mass' problem [8]. It compares the observed rotation curves of galaxies with the ones postulated from the visible matter of the same galaxies and finds that they are not agreeing. To make them agree, more invisible mass has to be added to the postulation. With this example, we can truly see that dark matter is not perceivable through 'light' directly but only through the gravitational imprint it leaves. This indicates that it does not interact electromagnetically and is therefore not directly visible through classical telescopes. We affiliate it with matter because of its gravitational imprint on the observations.

Besides this evidence, there is other like galaxy clusters and the large-scale structure, gravitational lensing, the bullet cluster, etc., see [28] and [29] for a well-written and detailed overview. The  $\Lambda$ -CDM model describes dark matter as non-baryonic, cold, dissipationless and collisionless (see [10] and [21]). In other words, it does not consist of protons and neutrons (non-baryonic), its velocity is far below the speed of light (cold), it can not lose energy by emitting photons (dissipationless) and the dark matter particles do not interact with each other or ordinary matter in any other way than gravitationally (collisionless).

Cold dark matter is the nowadays favored model for dark matter because it is

in general agreement with the observations of the large-scale structure. The idea is that dark matter 'clumps' together under its gravitational attraction to form it. This agrees with our general concept of how the universe evolved from a smooth initial state to the 'lumpy' structure we find today [3]. Still, the model of cold dark matter faces certain challenges, which makes it questionable. There are the core-cusp problem, the missing satellite problem, the angular momentum catastrophe, the disk of satellite problem and the small scale crisis. A nice overview of those is given in [24] and [33].

## 2.2 Dark Matter Density Profiles and SIDM Halos

The missing mass problem can be solved by introducing the concept of dark matter halos. A dark matter halo is a structure of dark matter which is decoupled from the cosmic expansion and gravitationally bound. Often those halos contain a galaxy or a galaxy cluster of ordinary matter while being a lot larger than the enclosed structure. Since they explain the observation, rotation curves are sometimes referred to as evidence for dark matter halos (see Fig. 2).

It is of particular interest for detection experiments how the dark matter mass is distributed across the halo. One of the most commonly used mass/density profiles for CDM is the Navarro-Frenk-White (NFW) profile. It fits a density function to dark matter halos and was identified through analyzing N-body simulations [16]. The function is given in (1) and relies on only two fitting parameters  $r_s$  and  $\rho_s$ , which make it a simple expression.

$$\rho(r) = \frac{\rho_s}{\frac{r}{r_s} \left(1 + \frac{r}{r_s}\right)^2} \quad (1)$$

The NFW profile describes a density distribution with an increasing density towards the inner region and is therefore referred to as a cored density profile (see e.g. [9]). Another cored density profile is the Hernquist profile. The corresponding density function is given as [12]:

$$\rho(r) = \frac{M a}{2\pi r} \frac{1}{(a+r)^3} \quad (2)$$

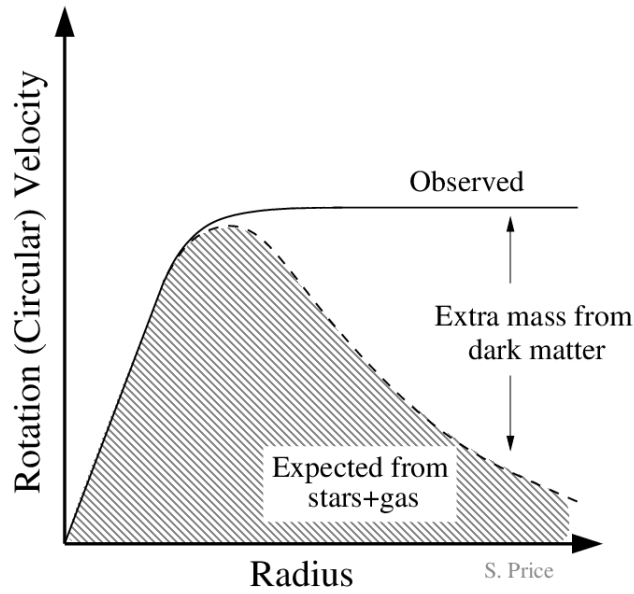


Figure 2: The 'Missing mass' problem: Contributions from ordinary matter to the circular velocity do not explain the observed circular velocity. To solve this discrepancy another form of non-visible matter is introduced: dark matter. (Reprinted from: [26])

Where  $a$  describes a scale length and  $M$  the total dark matter mass. We rewrite this equation to compare it with (1)

$$\rho(r) = \frac{\rho_0}{\frac{r}{a} \left(1 + \frac{r}{a}\right)^3}, \quad (3)$$

where we defined  $\rho_0 \equiv M/(2\pi a^3)$ . Like the NFW profile the Hernquist profile also only relies on two fitting parameters. A length scale  $a$  and a density scale  $\rho_0$ . It becomes clear that the main difference between the cored profiles is the exponent of the bracket term. This influences the behavior of the profile in the outer regions. Aside from these two profiles, others assume a finite core, i.e. an inner region with a constant density. One of them is the pseudo-isothermal profile [11] and its density function is given as:

$$\rho(r) = \frac{\rho_0}{\left(1 + \frac{r}{r_c}\right)^2} \quad (4)$$

Again, this function needs two fitting parameters  $r_c$  and  $\rho_0$ . For a general comparison of the profiles see Fig. 3.

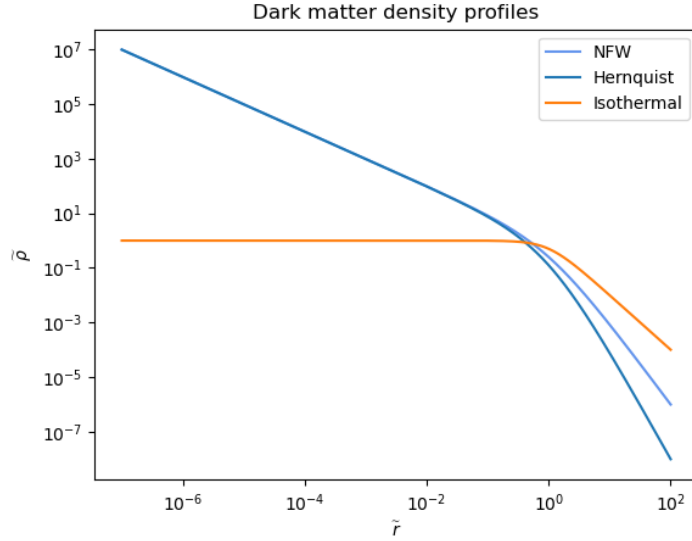


Figure 3: Original density profiles: We present the three discussed dark matter density profiles (NFW, Hernquist and Isothermal). This plot uses dimensionless units and the same fitting parameters for all three curves. For the inner regions, the flat behavior of the Isothermal profile is visible, as well as the identical behavior of NFW and Hernquist profiles. In the outer regions, the profiles become distinguishable and show different behavior.

The NFW profile is a good approximation for halo simulations of collisionless dark matter and different halo masses and redshifts in their equilibrium (virialized) state. It is also quite successful, when compared to observational data of large structures like galaxy clusters (see e.g. [19]). That is why we choose this profile for further consideration but will discuss the results for the other two as well. Still, this model is not perfect and has cases and regions where it does not describe the observation.

The problem we want to focus on is the core-cusp or ‘cuspy’ halo problem [33]. It is observed that the density profile of the inner regions (the core) of a dark matter halo is less dense than postulated from cold dark matter simulations. There are different approaches to solving this discrepancy between observation and simulation (see [15]). One way is to investigate if dark matter models different from the CDM model reproduce the observations. A promising model is the one of self-interacting dark matter (SIDM) [33]. In SIDM models dark matter particles scatter with each other and exchange energy and momentum. Those scatterings are characterized by the self-interaction cross-section. For the inner regions of dark matter halos, SIDM particle encounters are more likely and eventually thermalize the core (see Fig. 4). The so produced isothermal density profile solves the core cusp problem and is a natural feature of SIDM models (see e.g. [27]).

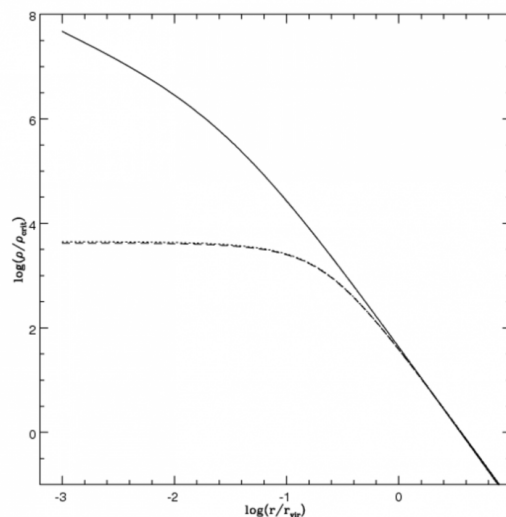


Figure 4: The core cusp problem: Simulations of CDM produce increasing densities for small radii. On the other hand observations indicate that the profile is rather flat in the inner regions of the halo. The straight line represents a typical NFW profile (corresponding to a CDM model) and the dashed line a profile obtained from SIDM simulations. The SIDM model reproduces the observed behaviour better than the CDM model. (Reprinted from: [23])

### 2.3 Dark Matter Density Spike

Almost all large galaxies host a massive central black hole. The presence of this mass could alter the dark matter distribution and eventually lead to overdensities in the inner halo regions. In the dark matter density profile, this additional attractive force leads to a density spike. Dark matter spikes are of particular interest since recent studies seek methods to investigate the nature of dark matter through gravitational waves (see e.g. [4]).

The density profiles of dark matter halos around a central black hole were examined in a very prominent paper by Gondolo and Silk [9]. Under the assumption that the black hole grew adiabatically, they studied the phase-space distribution. Through their semi-analytical approach to the system, Gondolo and Silk were able to find a generic expression for the density profile around the black hole from the phase space distribution. This was the first work that predicted the dark matter density spike. They considered two types of density profiles, either with a finite core or with an inner cusp. For finite core models, the prediction is a spike slope of  $\gamma_{sp} = 3/2$  in log-log space (independent of the exact model), while for cuspy profiles the spike slope depends on the initial slope  $\gamma$  of the profile in the inner region (see Fig. 5).

To generalize the problem they fitted each considered cuspy profile to a single power-law profile

$$\rho(r) = \rho_0 \left( \frac{r}{r_0} \right)^{-\gamma}, \quad (5)$$

with  $0 \leq \gamma \leq 2$ . In this fit the NFW and the Hernquist profile correspond to  $\gamma = 1$ .

Then the spike slope follows from [9] as

$$\gamma_{sp} = \frac{9 - 2\gamma}{4 - \gamma}. \quad (6)$$

Finally, the prediction for the spike slope of Hernquist and NFW profiles is  $\gamma_{sp} = 7/3$ .

As a check if observed behavior is really corresponding to a dark matter spike caused by the black hole, one can compare its position to the so-called spike

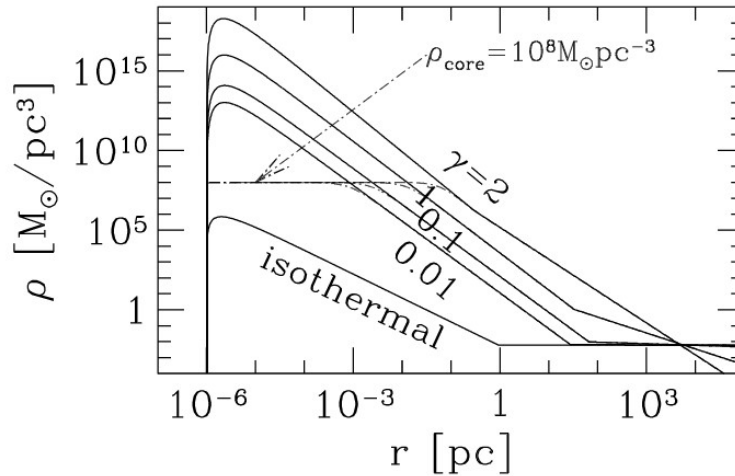


Figure 5: The resulting density spike found by Gondolo and Silk: The slope of the spike is independent of the model for finite core profiles (e.g. isothermal profile) and depends on the initial slope of the density for cuspy profiles. (Reprinted from [9])

radius  $r_{sp}$ . The spike radius is an approximation for the region, where the gravitational influence of the black hole could concentrate dark matter to form a spike (for further details see e.g. [6]). It is empirically defined as

$$r_{sp} \approx 0.2r_h, \quad (7)$$

where  $r_h$  is the radius within which the gravitational pull from the black hole dominates. It is approximately obtained by solving the integral

$$M(< r_h) = 4\pi \int_0^{r_h} \rho(r)r^2 dr = 2M_{BH}, \quad (8)$$

for  $r_h$ . With the spike radius, it is possible to divide the system into two parts. These are the spike region which is within the spike radius and the outer region which is outside the spike radius.

## 2.4 Aim and Structure of this Thesis

The goal of this work is to find if the spike in the density profile can be computed numerically with the gravothermal fluid model for self-interacting dark matter, determine its slope and compare it with semi-analytical predictions.

The structure of this thesis is the following. First I introduce the Lambda-CDM-Model and establish the importance of studying dark matter models, in particular self-interacting dark matter. Then I am going to lay out the theoretical foundation of the considered fluid model for self-interacting dark matter and extend it to apply it to our system. Next, I will discuss the numerical implementation of the model and present the obtained results. Finally, I am going to summarize my work and provide an outlook for possible future research.

### 3 Theoretical Foundations

The theoretical model used to describe the time evolution of the dark matter halo is the **gravothermal fluid model**. In this section, I will introduce the original gravothermal fluid model and discuss how the thermal conductivity is incorporated. Then I will discuss how the model needs to be modified if a central massive black hole is added to the system and discuss how the method of Lagrangian Zones simplifies the computation.

#### 3.1 The Gravothermal Fluid Model

The gravothermal fluid model is used to describe systems consisting of a self-gravitating heat-conducting fluid. Being first imposed in 1980 by Lynden-Bell and Eggleton [14], its original purpose was to describe the evolution of gas spheres. However, the model proves to work sufficiently well on stellar hydrodynamics (see e.g. [5]) and self-interacting dark matter (see [2]). The application on the latter is the main goal of this thesis.

The gravothermal fluid model relies on four equations, which arise from conservation of mass, hydrostatic equilibrium, heat conduction and the first two fundamental laws of thermodynamics. For simplicity of the calculations, we will consider spherical symmetrical systems. In the following sections, I will justify the usage and sketch the derivation of those four equations. A more complete and mathematically rigorous derivation of the equations can be found in [22].

##### Conservation of Mass

This first equation follows directly from the integral definition of the mass.

$$M(r') = 4\pi \int_0^{r'} \rho(r)r^2 dr. \quad (9)$$

Note that  $M(r)$  is the total dark matter mass within radius  $r$  and  $\rho(r)$  is the density profile of the dark matter. To use this equation in a numerical implementation it proved to be handy to rewrite it in differential form. This leads to our first gravothermal equation

$$\frac{\partial M}{\partial r} = 4\pi\rho(r)r^2. \quad (10)$$

### Hydrostatic Equilibrium

Obtaining the second gravothermal equation involves more derivation steps. Presented here is a mere sketch of the derivation. To start, one has to combine the Poisson equation of a gravitational potential (11) with the conservation equation obtained before (10). This gives an expression for the body acceleration (per unit mass);

$$\nabla^2\phi = \frac{1}{r^2} \frac{\partial}{\partial r} \left( r^2 \frac{\partial\phi}{\partial r} \right) = 4\pi G\rho \Leftrightarrow \frac{\partial\phi}{\partial r} = \frac{GM}{r^2}. \quad (11)$$

The next step is to use the Euler momentum equation (12), bearing in mind that a fluid in hydrostatic equilibrium has no flow/macroscopic velocity ( $\mathbf{v} = 0$ ). Here,  $p$  denotes the mechanic pressure.

$$\frac{\partial\mathbf{v}}{\partial t} + (\mathbf{v} \cdot \nabla) \mathbf{v} = 0 = -\frac{\nabla p}{\rho} - \nabla\phi \Leftrightarrow \nabla p = -\rho\nabla\phi \quad (12)$$

By plugging in the previously obtained expression in (11), the second gravothermal equation of hydrostatic equilibrium is obtained:

$$\frac{\partial p}{\partial r} = -\frac{GM\rho}{r^2}. \quad (13)$$

### Heat Conduction

The third equation considers the heat flux  $q$  within the system, which depends on the temperature gradient  $\nabla T$  and a conductivity coefficient  $\kappa$ . Sometimes this is called Fourier's law of heat conduction. It is useful to write it in terms of the luminosity  $L$  per spherical surface as discussed in [14];

$$q = \frac{L}{4\pi r^2} = -\kappa \frac{\partial T}{\partial r}. \quad (14)$$

The explicit form of this equation depends on the nature of the conduction. For ordinary heat diffusion, it will rely on the mean free path between collisions. This is of particular interest for the examined system and will be discussed in section 3.2.

### Laws of Thermodynamics

For the fourth equation, the first and second law of thermodynamics need to be evaluated for the system. To start the second law is written in terms of specific quantities, e.g. the specific entropy  $s = S/M$ ;

$$Tds = \frac{1}{\rho V}dQ. \quad (15)$$

To derive our equation, the time derivative is taken, which is a Lagrangian derivative (denoted by the  $M$ ). The Lagrangian derivative follows a certain mass parcel. Lagrangian zones and their application in this thesis will be discussed in section 3.4.

$$T \left( \frac{\partial s}{\partial t} \right)_M = \frac{1}{\rho V} \left( \frac{\partial Q}{\partial t} \right)_M \quad (16)$$

But  $Q/V$  is simply an energy density  $u$ , therefore it follows the conservation equation of energy:

$$\frac{\partial u}{\partial t} + \nabla \mathbf{q} = 0. \quad (17)$$

Now, this is used to rewrite (16). For the spherical symmetrical case and by inserting the definition of the luminosity, we get:

$$T \left( \frac{\partial s}{\partial t} \right)_M = -\frac{1}{\rho} \nabla \mathbf{q} = -\frac{1}{4\pi\rho r^2} \frac{\partial L}{\partial r}. \quad (18)$$

Starting from the first law of thermodynamics and rewriting in terms of specific energy  $u$  and entropy  $s$  and then solving for  $ds$  gives:

$$ds = \frac{1}{T} \left. \frac{\partial u}{\partial T} \right|_p dT + \left[ \frac{1}{T} \left. \frac{\partial u}{\partial p} \right|_T - \frac{p}{T\rho^2} \right] d\rho. \quad (19)$$

The specific energy  $u$  of an ideal gas reads as:

$$u = \frac{3}{2} \frac{k_B T}{m}. \quad (20)$$

Now (20) is inserted in (19), which is then integrated and gives the expression for  $s$ :

$$s = \frac{k_B}{m} \ln \left( \frac{T^{3/2}}{\rho} \right). \quad (21)$$

Finally, we can plug this equation (21) into (18).

$$\frac{\partial L}{\partial r} = -4\pi\rho r^2 v^2 \left( \frac{\partial}{\partial t} \right) \Big|_M s \quad (22)$$

Now with (28) this is written in terms of  $v$ . This gives the fourth equation for the gravothermal fluid model:

$$\frac{\partial L}{\partial r} = -4\pi\rho r^2 v^2 \left( \frac{\partial}{\partial t} \right) \Big|_M \ln \frac{v^3}{\rho}. \quad (23)$$

### 3.2 Thermal Conductivity

To determine the explicit form of (14), the elementary theory of thermal conductivity of gases [14] is used. The ansatz is to determine the heat flux by considering the positive and negative flux of heat/energy through an imaginary surface.

$$q = \frac{1}{2} (q_{in} + q_{out}), \quad (24)$$

where the energy flux can be understood as the particle flux through the surface times the average energy per particle. The particle flux is given by the number density  $n$  times the quotient of mean free path  $\lambda$  and the time between collisions  $\tau$ . The flux then reads as:

$$q = \frac{3 k_B n \lambda}{4 \tau} (-T_{in} + T_{out}), \quad (25)$$

where  $T_{in}$  and  $T_{out}$  denote the temperature just above/below the imaginary surface. They can be approximated as [22] suggests with the expression in (26). This is because the deviation from the surface temperature  $T(r)$  is the partial derivative times the mean free path  $\lambda$  and the effective impact parameter  $b$ , which can be calculated from transport theory.

$$T_{in,out} = T(r) \pm b\lambda \frac{\partial T}{\partial r} \quad (26)$$

With (26) and inserting that  $n = \rho/m$  the expression (25) becomes

$$q = -\frac{3}{2} \frac{\lambda^2}{\tau} b \rho \frac{\partial}{\partial r} \left( \frac{k_B T}{m} \right). \quad (27)$$

To get rid of the temperature dependence, the partial derivative in the last term has to be rewritten. To do so we can use the equipartition theorem of an ideal gas

$$\frac{3}{2} k_B T = \frac{1}{2} m \mathbf{v}^2 \Leftrightarrow \frac{3 k_B T}{m} = \mathbf{v}^2. \quad (28)$$

Now, this is put in terms of a one-dimensional velocity dispersion  $v$ .

$$v^2 \equiv \langle v_i^2 \rangle = \frac{1}{3} \langle \mathbf{v}^2 \rangle \quad (29)$$

This leads us to the temperature-independent formulation of the luminosity/heat flux

$$\frac{L}{4\pi r^2} = -\frac{3}{2} \frac{b \lambda^2}{\tau} \rho \frac{\partial v^2}{\partial r}. \quad (30)$$

This expression holds for monatomic fluids without loss of generality. To apply it to the SIDM fluid which is considered in this work, two cases for the mean free path  $\lambda$  need to be examined. For this  $\lambda$  needs to be compared with a characteristic length scale  $H$  (gravitational scale height), which is the local Jeans length  $r_J(r)$  (31) for this system [2]. It can be imagined as the length over which the gravitational pull decreases/increases by a factor of  $e$ .

$$r_J^2(r) \equiv \frac{v^2}{4\pi G \rho(r)} \quad (31)$$

The first case treats ordinary heat diffusion, where the mean free path is much smaller than the size of the system (e.g.  $\lambda \ll H$ ). We call this the short mean free path (SMFP) case, and the relation  $v = \lambda/\tau$  applies. In this limit the luminosity equation becomes

$$\frac{L}{4\pi r^2} = -\frac{3}{2} b \lambda v \rho \frac{\partial v^2}{\partial r}. \quad (32)$$

The other case considers that for dilute gravothermal systems the mean free path is much larger than the scale height (e.g.  $\lambda \gg H$ ). One could imagine a

mass to make several orbits and move around by a typical distance comparable to a Jeans length between interactions. The time between these interactions is not the  $\tau$  introduced before but rather a relaxation time  $t_r$ . It is introduced in [14], while the explicit form which is used here and a more detailed discussion of the timescales is given in [2]. This case is called the long mean free path (LMFP) limit [31] and the luminosity equation can be approximated as

$$\frac{L}{4\pi r^2} = -\frac{3}{2}b\rho\frac{H^2}{t_r}\frac{\partial v^2}{\partial r}. \quad (33)$$

To fully cover the real behavior of the system, both cases need to be taken into account. By interpolating as suggested in [2], the two luminosity equations are combined into one (34), which correctly reduces to (33) in the LMFP limit and (32) in the SMFP limit. Following the work of [17] a calibration parameter  $C$  is added to match the observations of CDM halos in the LMFP regime. This parameter  $C$  is used to control the impact of the SMFP and LMFP regimes on the system's behavior as a whole.

$$\frac{L}{4\pi r^2} = -\frac{3}{2}b\rho v \left[ \frac{1}{\lambda} + \frac{1}{C} \frac{vt_r}{H^2} \right]^{-1} \frac{\partial v^2}{\partial r} \quad (34)$$

Since  $\lambda$  is a collisional scale for the mean free path, it can be written as  $\lambda = 1/(\rho\sigma)$  in the SMFP regime ( $\sigma$  denotes the self-interaction cross-section of the dark matter particles per unit mass). For the LMFP regime [2] and [17] define  $t_r \equiv 1/(a\rho v\sigma)$ , where  $a$  "is a coefficient relevant for hard-sphere scattering of particles with a Maxwell-Boltzmann velocity distribution" [2]. Plugging in those relations yields the final form of the luminosity equation:

$$\frac{L}{4\pi r^2} = -\frac{3}{2} \left[ \frac{\sigma}{bv} + \frac{1}{C} \frac{1}{H^2} \frac{1}{a\rho^2 v\sigma} \right]^{-1} \frac{\partial v^2}{\partial r} \quad (35)$$

### 3.3 Central Black Hole Modification

For this thesis, the well-tested gravothermal fluid model is extended by placing a black hole in the center of the halo. The underlying detailed discussion is given in [30]. In this section, I will explain the key arguments and how they lead to alterations in the model.

### Black Hole Mass

What is meant by "placing a black hole in the center of the halo" is adding a point-like mass to the system. Of course, this does not cover the full reality of a physical black hole. Properties like mass accretion and growth would possibly make a sizable impact on the evolution at the regarded time scales. This is also the case for relativistic corrections (see e.g. [30]) Implementing those could be part of future work.

The main impact on the model is in the second gravothermal fluid equation for the hydrostatic equilibrium. With the addition of the black hole mass, the gravitational potential increases. This leads to a new hydrostatic equilibrium equation

$$\frac{\partial p}{\partial r} = -\rho G \frac{M + M_{BH}}{r^2}. \quad (36)$$

Interesting to note here is, that the first equation of hydrostatic equilibrium for mass conservation is not altered. This is because the black hole mass is a constant addition and therefore would vanish in the partial derivative in (10).

### Gravitational Scale Height

The second change in the model is in the luminosity equation (35) or, more precisely, in the LMFP limit. Until now, the gravitational scale height  $H$  was set by the Jeans length  $r_J$ . With adding the black hole, the inner regions are dominated by its gravitational pull and form a kind of cusp. [30] argues that in this region the gravitational scale height is comparable to the orbital radius  $r$  (with  $r \ll r_J$ ). The scale height for the whole system is then given by (37).

$$H = \min(r, r_J) \quad (37)$$

This can be plugged into (35) and gives the new luminosity equation describing the system with black hole (38).

$$\frac{L}{4\pi r^2} = \begin{cases} -\frac{3}{2} \left[ \frac{\sigma}{bv} + \frac{1}{C} \frac{1}{r^2} \frac{1}{a\rho^2 v\sigma} \right]^{-1} \frac{\partial v^2}{\partial r} & r < r_J \\ -\frac{3}{2} \left[ \frac{\sigma}{bv} + \frac{1}{C} \frac{4\pi G}{a\rho v^3\sigma} \right]^{-1} \frac{\partial v^2}{\partial r} & r > r_J \end{cases} \quad (38)$$

With (10), (36), (38) and (23) we have the complete set of equations describing the gravothermal fluid model with a central black hole.

### 3.4 Lagrangian Zones

In this thesis, the usage of fluid models and fluid dynamics in general plays a fundamental role. We employ the principles of fluid dynamics as tools to simplify and enable us to do meaningful computations. Of the highest importance are two tools, the previously discussed gravothermal fluid model (especially the theory of heat conduction and thermal conductivity) and the Lagrangian (or material) coordinate system. In this subsection, I want to explain the general idea of the Lagrangian zones and emphasize how useful they have proven to be for our work. The general topic consists of a whole underlying theory and was extensively studied. Limiting myself to the key points, see [25] for an in-depth explanation, which is the main source for this discussion.

In general, there are two ways to observe a fluid flow. The first one is to define an (Eulerian) control volume, which is fixed in space, and describe the fluid properties in this volume. It allows fluid flow in and out of the volume. The other way is by defining a (Lagrangian) material volume. One can imagine it in a way, that the fluid is divided into small portions that are carried along with the flow (see Fig. 6). Either one or multiple parcels make up a control volume and we try to describe the position and thermodynamical properties of the volume. "The continuum model assumes that either a material volume or a control volume may be made as small as is necessary to resolve the phenomenon of fluid flow." [25]

The terms control volume, Lagrangian volume and Lagrangian zone are used synonymously. These zones divide the fluid into small parcels which are fixed to the included mass. Since the parcels cannot pass through each other or the boundary the mass of each parcel is kept constant. As the parcel moves with the fluid flow the position and its thermodynamical properties will change. In a way, we are 'moving along' with the flow instead of observing it from the outside.

At this point, we can already grasp the possible interplay of Lagrangian zones

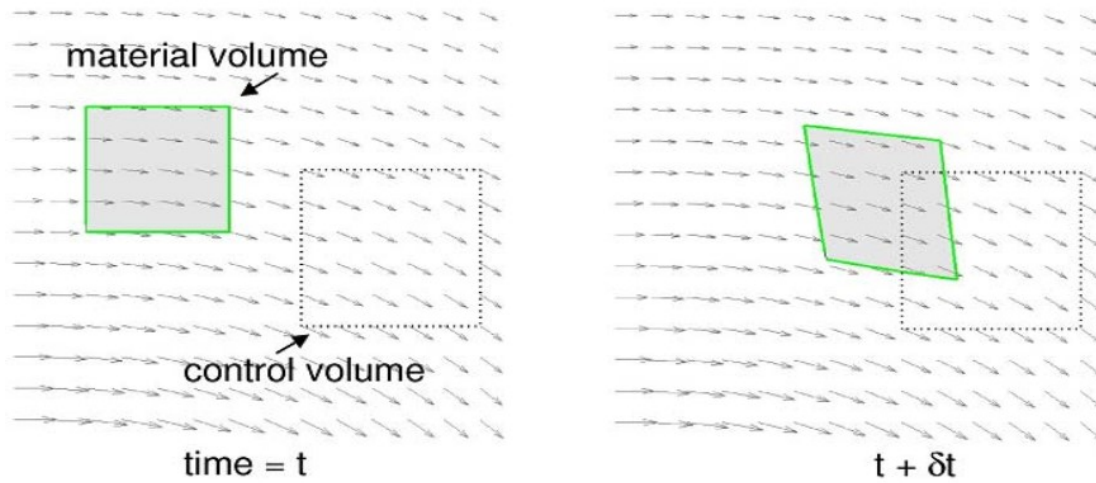


Figure 6: Material volumes follow certain mass points, not allowing any flow in or out the volume, while position, size and thermodynamical properties change. Control volumes are fixed in space and allow fluid flow through the volume. (Reprinted from: [25])

and the gravothermal fluid model. By using these zones, the first gravothermal equation of mass conservation (10) is always fulfilled, since the mass of each zone is constant and we do not 'lose' zones. Another thing to note is that the fourth gravothermal fluid equation (23) contains a Lagrangian derivative that follows a certain mass parcel e.g. a Lagrangian zone. Later on, we will argue how with the Lagrangian zones and another consideration the equation as a whole is always fulfilled.

I will explain in detail how the Lagrangian zones are used for evolving the halo in section 4.3.

## 4 Numerical Approach

In this section, I will discuss how the gravothermal fluid model is implemented numerically. By following the approach I will present, it will be possible to simulate the evolution of SIDM halos for short and long times. As mentioned in the introduction this is particularly interesting to examine the nature of dark matter by comparing the simulation's results to observations.

The general ideas of the implementation of the model are well discussed in [22]. For this thesis, I am following the work of [17] and modify their code by implementing a central black hole. The theoretical framework on how to extend the gravothermal fluid equations to do so is explained in [30].

### 4.1 Dimensionless equations and quantities

To implement the model numerically the four gravothermal fluid equations need to be rewritten in terms of dimensionless quantities. The general ansatz to do so is as follows: A quantity  $x$  is divided by a fiducial quantity *of comparable scale* of the system  $x_0$  to yield a dimensionless quantity  $\tilde{x}$

$$\tilde{x} = \frac{x}{x_0} \Leftrightarrow x = \tilde{x} \cdot x_0. \quad (39)$$

For reasons of consistency one has to decide on a set of fiducial quantities beforehand and then perform the transformation to dimensionless equations. The code that we want to extend uses the set given in [7]. The fiducial quantities are:

$$\begin{aligned} r_0 &= r_s & \rho_0 &= \rho_s \\ M_0 &= 4\pi\rho_s r_s^3 & \sigma_0 &= (\rho_s r_s)^{-1} \\ \nu_0 &= (4\pi G \rho_s)^{1/2} r_s & L_0 &= (4\pi)^{5/2} G^{3/2} \rho_s^{5/2} r_s^5 \\ t_0 &= (4\pi G \rho_s)^{-1/2} \end{aligned}$$

Table 1: Fiducial quantities

It is easy to see, that all quantities are built upon  $r_s$  and  $\rho_s$ . These are the fitting parameters of the NFW profile (1) and vary from halo to halo. Therefore

it is necessary to pick them carefully for each system. Choosing unrealistic parameters eventually leads to severe errors in numerical computation.

The quantities from table 1 are plugged into the gravothermal equations (10), (36), (35) and (23) following the method in (39). After canceling out constants, this yields the dimensionless gravothermal equations:

$$\frac{\partial \tilde{M}}{\partial \tilde{r}} = \tilde{r}^2 \tilde{\rho} \quad (40)$$

$$\frac{\partial(\tilde{\rho}\tilde{v}^2)}{\partial \tilde{r}} = -\tilde{\rho} \frac{\tilde{M} + \tilde{M}_{BH}}{\tilde{r}^2} \quad (41)$$

$$\frac{\partial \tilde{L}}{\partial \tilde{r}} = -\tilde{r}^2 \tilde{\rho} \tilde{v}^2 \frac{\partial}{\partial \tilde{t}} \ln \left( \frac{\tilde{v}^3}{\tilde{\rho}} \right) \quad (42)$$

$$\tilde{L} = -\frac{3}{2} \tilde{r}^2 \left[ \frac{\tilde{\sigma}}{b\tilde{v}} + \frac{1}{C} \frac{1}{\tilde{H}^2} \frac{1}{\tilde{\rho}^2 \tilde{\sigma} \tilde{v} a} \right]^{-1} \frac{\partial \tilde{v}^2}{\partial \tilde{r}}. \quad (43)$$

Note that in (43) the general case for  $H$  is considered, since for both cases in (38)  $H$  is of unit length.

## 4.2 Discretization and Initial Data

To compute the evolution of the system, the halo is divided in  $N$  spherical shells which are equally spaced in log space with radii  $r_{i=1..N}$ . Then the gravothermal equations are discretized. This essentially means that the partial derivatives are written as finite differences of neighbouring shells and all quantities are evaluated at the discrete radii (e.g.  $\tilde{M}(\tilde{r}_i) \equiv \tilde{M}_i$ ). For all extensive quantities (such as mass, volume, ect.) this is trivial. On the other hand the intensive quantities (such as density, internal energy, ect.) need to be treated differently. Following the work of [22] we define them as the average value within the 'i'-th shell, so that for example  $\tilde{\rho}_i$  denotes the value at  $(\tilde{r}_{i-1} + \tilde{r}_i) / 2$  (see Fig. 7). Now to evaluate  $\tilde{\rho}_i$  at  $\tilde{r}_i$  one just has to take the average of the density in the 'i'-th and 'i-1'-th shell,  $(\tilde{\rho}_{i-1} + \tilde{\rho}_i) / 2$ .

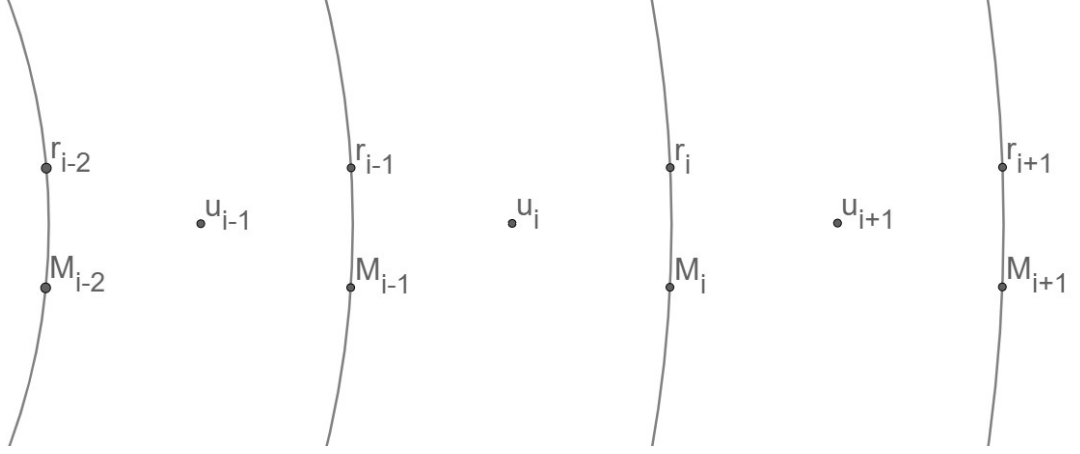


Figure 7: Example of where intensive and extensive quantities are defined. The extensive quantities like mass are defined at the corresponding shell radius. The intensive quantities like internal energy denote the average value within a shell. They are defined at the mid of the corresponding shell.

To evolve the halo an initial data frame of all quantities is necessary. To produce this data frame we assume an initial NFW profile (1) and start by computing  $\tilde{M}_i$ . There is an analytical expression for the enclosed mass of radius  $\tilde{r}_i$  (44)

$$\tilde{M}_i = \int_0^{\tilde{r}_i} \tilde{\rho} r^2 d\tilde{r} = \int_0^{\tilde{r}_i} \tilde{r}^{-1} (1 + \tilde{r})^{-2} \tilde{r}^2 d\tilde{r} = -\frac{\tilde{r}_i}{1 + \tilde{r}_i} + \ln(1 + \tilde{r}_i). \quad (44)$$

Note that the typical factor of  $4\pi$  for spherical integration drops out since we are dealing with dimensionless quantities. With the enclosed mass of each shell, we can compute the density  $\tilde{\rho}_i$  within the shell and then the pressure  $\tilde{p}_i$  (Note that for the latter we present an integral, but there is an analytical solution too).

$$\tilde{\rho}_i = \frac{\tilde{M}_i - \tilde{M}_{i-1}}{\tilde{V}_i - \tilde{V}_{i-1}} = 3 \frac{\tilde{M}_i - \tilde{M}_{i-1}}{\tilde{r}_i^3 - \tilde{r}_{i-1}^3} \quad (45)$$

$$\tilde{p}_i = \int_{(\tilde{r}_{i+1} + \tilde{r}_i)/2}^{\infty} \frac{\tilde{\rho} \tilde{M}}{\tilde{r}^2} d\tilde{r} \quad (46)$$

To complete the initial data frame we can use  $\tilde{p} = \tilde{\rho} \tilde{v}^2$  (which follows from the ideal gas law) to compute the velocity dispersion  $\tilde{v}$  and  $\tilde{u} = 3\tilde{v}^2/2$  (see

(20), (28) and (29)) to compute the internal energy  $\tilde{u}$ . Finally with all of those quantities the luminosity  $\tilde{L}$  is calculated. For clarity we recognize the bracket in (43) as the thermal conductivity  $\tilde{\kappa}$  and write the partial derivative in terms of  $\tilde{u}$ :

$$\tilde{L} = -\tilde{r}^2 \tilde{\kappa} \frac{\partial \tilde{u}}{\partial \tilde{r}} \quad (47)$$

Since almost all quantities in  $\tilde{\kappa}$  are intensive, we can treat  $\tilde{\kappa}$  itself as an intensive quantity. The only extensive quantity in  $\tilde{\kappa}$  is  $H$  for the case  $r \gg r_J$ , but this is easily solved by using the midpoints of the shells (e.g.  $(\tilde{r}_{i+1} - \tilde{r}_i) / 2$ ). The discretized luminosity equations reads:

$$\tilde{L}_i = -\tilde{r}_i^2 \frac{\tilde{\kappa}_{i-1} + \tilde{\kappa}_i}{2} \frac{2(\tilde{u}_{i+1} - \tilde{u}_i)}{\tilde{r}_{i+1} - \tilde{r}_{i-1}} \quad (48)$$

With the thermal conductivity  $\tilde{\kappa}$ :

$$\tilde{\kappa}_i = \begin{cases} \left[ \frac{\tilde{\sigma}}{b\tilde{v}_i} + \frac{1}{aC} \frac{1}{\tilde{\rho}_i^2 \tilde{v}_i \tilde{\sigma}} \left( \frac{2}{\tilde{r}_{i+1} - \tilde{r}_i} \right)^2 \right]^{-1} & r < r_J \\ \left[ \frac{\tilde{\sigma}}{b\tilde{v}_i} + \frac{1}{aC} \frac{1}{\tilde{\rho}_i \tilde{v}_i^2 \tilde{\sigma}} \right]^{-1} & r > r_J \end{cases} \quad (49)$$

Now that all the initial properties of the system are obtained, we can start the time evolution.

### 4.3 Time Evolution

The key principle to evolving the system in time is to conduct a small portion of heat between the Lagrangian zones (i.e. change the internal energy). Since the mass is kept constant in those zones, the thermodynamical properties need to be adjusted to maintain the hydrostatic equilibrium. Once hydrostatic equilibrium is achieved, the next energy portion can be conducted and the process repeats [17] (see Fig. 8).

#### Heat Conduction and Timesteps

The amount of energy conducted in one step  $\Delta \tilde{u}$  is given through the luminosity per mass times a timestep  $\Delta \tilde{t}$  and is given as

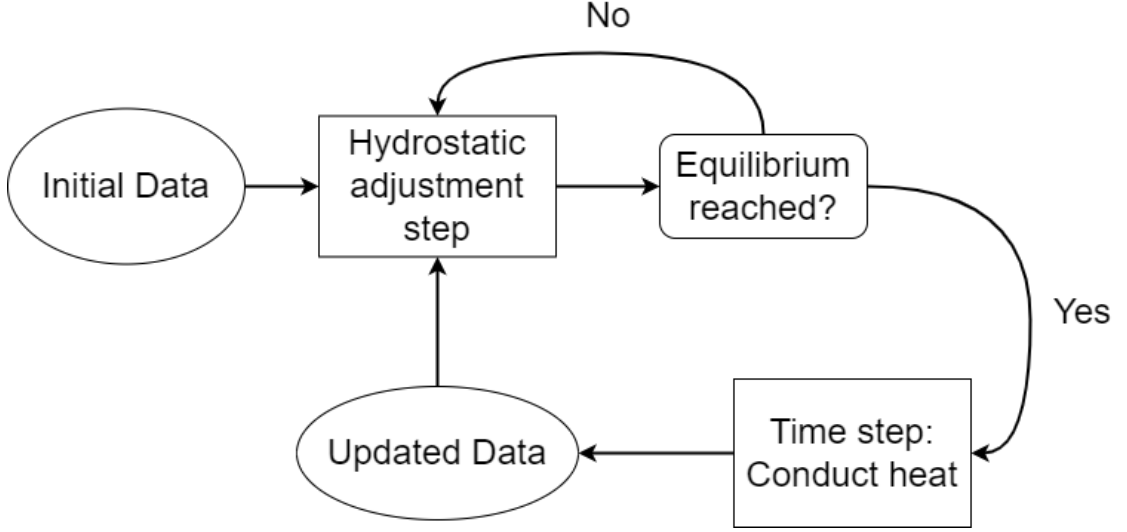


Figure 8: Flowchart of implementation: The code starts with an initial data frame and drives the system into an equilibrium state. Once the hydrostatic equilibrium is reached, a timestep is taken and heat is conducted within the system. Through the increase of internal energy in the shells, the thermodynamic quantities are altered and the system is driven out of equilibrium. With the updated data frame the process is repeated.

$$\Delta\tilde{u} = -\frac{\Delta\tilde{L}}{\Delta\tilde{M}}\Delta\tilde{t} \Leftrightarrow \Delta\tilde{u}_i = -\frac{\tilde{L}_i - \tilde{L}_{i-1}}{\tilde{M}_i - \tilde{M}_{i-1}}\Delta\tilde{t}. \quad (50)$$

This change in internal energy will alter the density of the mass shells. Therefore, we require that the timestep  $\Delta\tilde{t}$  is small, for the effect to be negligible. In terms of the internal energy this means that  $|\Delta\tilde{u}|/\tilde{u} \ll 1$ . The choice of the timestep and a general discussion of timescales is given in [2]. There are two ways of determining the timestep. The first one is to choose  $\Delta\tilde{t}$  to be the minimum local relaxation time  $t_r$  used in deriving (35) times a small  $\epsilon_{t_r}$ , as suggested by [17].

$$\Delta\tilde{t} = \epsilon_t \tilde{t}_r \quad (51)$$

The second way is to make sure the relative change in internal energy is small. To do so (50) is rewritten as:

$$\left| \frac{\Delta \tilde{L}}{\Delta \tilde{M}} \right| = \left| \frac{\Delta \tilde{u}}{\Delta \tilde{t}} \right| \quad (52)$$

Now we divide the internal energy  $\tilde{u}$  by the l.h.s. in (52) and obtain

$$\frac{\tilde{u}}{\left| \frac{\Delta \tilde{L}}{\Delta \tilde{M}} \right|} = \frac{\tilde{u}}{|\Delta \tilde{u}|} |\Delta \tilde{t}|. \quad (53)$$

Since the l.h.s. in (53) is just a number, we can set  $|\Delta \tilde{u}| / \tilde{u} \equiv \epsilon_t$ . After choosing a sufficiently small value for  $\epsilon_t$  ([17] suggests  $\epsilon_t = 10^{-4}$ ), the timestep  $\Delta \tilde{t}$  is directly calculated as:

$$\frac{\tilde{u}}{\left| \frac{\Delta \tilde{L}}{\Delta \tilde{M}} \right|} = \frac{1}{\epsilon_t} \Delta \tilde{t} \Leftrightarrow \Delta \tilde{t} = \left| \frac{\Delta \tilde{L}}{\Delta \tilde{M}} \right| \epsilon_t \quad (54)$$

Now one can either decide on one criterion for the timestep or just use the minimum of both to really secure that the evolution is sufficiently smooth, which is what we will use.

A change of internal energy always goes along with a change in the other thermodynamical properties, which are density and pressure. Since we choose the timestep in a way to make the change in density negligible, only the change in pressure needs to be taken into account. With  $\tilde{p} = \tilde{\rho} \tilde{v}^2$  and  $\tilde{u} = 3\tilde{v}^2/2$  we can write:

$$\tilde{u} = \frac{3}{2} \frac{\tilde{p}}{\tilde{\rho}} \quad (55)$$

From (55) follows directly (56), where we assume the density to be constant as discussed before. So the relative change in internal energy is the same as in pressure.

$$\frac{\Delta \tilde{u}}{\tilde{u}} = \frac{\Delta \tilde{p}}{\tilde{p}} \Leftrightarrow \Delta \tilde{p} = \frac{\Delta \tilde{u}}{\tilde{u}} \tilde{p} \quad (56)$$

Finally the pressure after the heat conduction is just  $\tilde{p} + \Delta \tilde{p}$ . The whole process has moved the system of Lagrangian zones out of the equilibrium state, which needs to be solved.

### Hydrostatic Equilibrium and the Tridiagonal Matrix Equation

The discrete form of the second gravothermal fluid equation of hydrostatic equilibrium from (41) is

$$\frac{\tilde{p}_{i+1} - \tilde{p}_i}{(\tilde{r}_{i+1} - \tilde{r}_{i-1}) / 2} = -\frac{\tilde{M}_i \tilde{\rho}_{i+1} + \tilde{\rho}_i}{\tilde{r}_i^2} \cdot \quad (57)$$

Here we see that it depends on pressure, density, mass and radial position of each shell. Therefore the alteration out of equilibrium caused by the heat conduction depends on the changes in those quantities. "To return the halo to hydrostatic equilibrium, we adjust the shell location  $\tilde{r}_i \rightarrow \tilde{r}_i + \Delta\tilde{r}_i$ , pressure  $\tilde{p}_i \rightarrow \tilde{p}_i + \Delta\tilde{p}_i$  and density  $\tilde{\rho}_i \rightarrow \tilde{\rho}_i + \Delta\tilde{\rho}_i$ " [17]. Inserting these adjustments into (57) gives an equation which fulfills the equilibrium state again [22]:

$$\frac{\tilde{p}_{i+1} + \Delta\tilde{p}_{i+1} - \tilde{p}_i - \Delta\tilde{p}_i}{(\tilde{r}_{i+1} + \Delta\tilde{r}_{i+1} - \tilde{r}_{i-1} - \Delta\tilde{r}_{i-1}) / 2} + \frac{\tilde{M}_i}{(\tilde{r}_i + \Delta\tilde{r}_i)^2} \frac{\tilde{\rho}_{i+1} + \Delta\tilde{\rho}_{i+1} + \tilde{\rho}_i + \Delta\tilde{\rho}_i}{2} = 0. \quad (58)$$

The goal is to find a correct set of adjustments. Now we want to eliminate the dependency on the changes in pressure and density in this equation so we only have the dependency on the change of shell location. We start by finding an expression for the change in dimensionless volume by writing the total derivative concerning  $\tilde{r}$  as a finite difference.

$$\frac{d\tilde{V}}{d\tilde{r}} = \frac{d}{d\tilde{r}} \left( \frac{1}{3} \tilde{r}^3 \right) \Rightarrow d\tilde{V} = \tilde{r}^2 d\tilde{r} \Rightarrow \Delta\tilde{V} = \tilde{r}^2 \Delta\tilde{r} \quad (59)$$

With the volume of a single shell  $\tilde{V}_i = (\tilde{r}_i^3 - \tilde{r}_{i-1}^3) / 3$  we obtain the expression for  $\Delta\tilde{V}_i$

$$\Delta\tilde{V}_i = \tilde{V}_i - \tilde{V}_{i-1} = \tilde{r}_i^2 \Delta\tilde{r}_i - \tilde{r}_{i-1}^2 \Delta\tilde{r}_{i-1}. \quad (60)$$

Next, we want to find the expression for the change in density. Again we start with the total derivative but this time concerning volume.

$$\frac{d\tilde{\rho}}{d\tilde{V}} = \frac{d}{d\tilde{V}} \left( \frac{\tilde{M}}{\tilde{V}} \right) = \tilde{M} \frac{d}{d\tilde{V}} \left( \frac{1}{\tilde{V}} \right) = -\frac{\tilde{M}}{\tilde{V}^2} = -\frac{\tilde{\rho}}{\tilde{V}} \Rightarrow d\tilde{\rho} = -\frac{\tilde{\rho}}{\tilde{V}} d\tilde{V} \Rightarrow \Delta\tilde{\rho} = -\frac{\tilde{\rho}}{\tilde{V}} \Delta\tilde{V} \quad (61)$$

By inserting the previously obtained expressions for  $\tilde{V}$  and  $\Delta\tilde{V}$ , we get an equation for  $\Delta\tilde{\rho}$  which only depends on  $\tilde{\rho}$ ,  $\tilde{r}$  and  $\Delta\tilde{r}$ :

$$\Delta\tilde{\rho}_i = -\tilde{\rho}_i \frac{\Delta\tilde{V}_i}{\tilde{V}_i} = -3\tilde{\rho}_i \frac{\tilde{r}_i^2 \Delta\tilde{r}_i - \tilde{r}_{i-1}^2 \Delta\tilde{r}_{i-1}}{\tilde{r}_i^3 - \tilde{r}_{i-1}^3}. \quad (62)$$

To find the expression for the change in pressure we keep the entropy of each Lagrangian zone fixed, so the process is adiabatic [2] and the third gravothermal fluid equation (42) is always fulfilled. For all adiabatic processes there is an adiabatic invariant  $pV^{5/3} = \text{const.}$  [22]. Therefore the total derivative concerning the volume is:

$$0 = \frac{d\tilde{p}\tilde{V}^{5/3}}{d\tilde{V}} = \tilde{V}^{5/3} \frac{d\tilde{p}}{d\tilde{V}} + \tilde{p} \frac{d\tilde{V}^{5/3}}{d\tilde{V}} = \tilde{V}^{5/3} \frac{d\tilde{p}}{d\tilde{V}} + \frac{5}{3} \tilde{p} \tilde{V}^{2/3} \Rightarrow d\tilde{p} = -\frac{5}{3} \tilde{p} \frac{d\tilde{V}}{\tilde{V}} \quad (63)$$

Again we discretize this as finite differences and insert the expressions for the volume to get the expression for the change in pressure only depending on  $\tilde{p}$ ,  $\tilde{r}$  and  $\Delta\tilde{r}$ :

$$\Delta\tilde{p}_i = -\frac{5}{3} \tilde{p}_i \frac{\Delta\tilde{V}_i}{\tilde{V}_i} = -5\tilde{p}_i \frac{\tilde{r}_i^2 \Delta\tilde{r}_i - \tilde{r}_{i-1}^2 \Delta\tilde{r}_{i-1}}{\tilde{r}_i^3 - \tilde{r}_{i-1}^3}. \quad (64)$$

Now with (64) and (62), the equation (58) only depends on the changes in shell position  $\Delta\tilde{r}_i$  and the initial data. This allows us to bring the system back into the equilibrium state by just finding a set of  $\Delta\tilde{r}_i$ . By multiplying with the denominators of the summands in (58) and rearranging the terms, we can write the equilibrium equation in the following form:

$$a_i \Delta\tilde{r}_{i-1} + b_i \Delta\tilde{r}_i + c_i \Delta\tilde{r}_{i+1} = -d_i \quad (65)$$

Where we neglect terms of order  $\mathcal{O}(\Delta\tilde{r}^2)$ , since throughout the evolution  $\Delta\tilde{r} \ll 1$ . This is satisfied by choosing the timestep sufficiently small. The coefficients  $a$ ,  $b$ ,  $c$  and  $d$  are:

$$a_i = \frac{3M_i \rho_i r_{i+1} r_{i-1}^2}{2r_i^3 - 2r_{i-1}^3} - \frac{3M_i \rho_i r_{i-1}^3}{2r_i^3 - 2r_{i-1}^3} - \frac{M_i \rho_i}{2} - \frac{M_i \rho_{i+1}}{2} - \frac{10p_i r_i^2 r_{i-1}^2}{r_i^3 - r_{i-1}^3} \quad (66)$$

$$b_i = -\frac{3M_i \rho_i r_i^2 r_{i+1}}{2r_i^3 - 2r_{i-1}^3} + \frac{3M_i \rho_i r_i^2 r_{i-1}}{2r_i^3 - 2r_{i-1}^3} + \frac{3M_i \rho_{i+1} r_i^2 r_{i+1}}{-2r_i^3 + 2r_{i+1}^3} - \frac{3M_i \rho_{i+1} r_i^2 r_{i-1}}{-2r_i^3 + 2r_{i+1}^3} + \frac{10p_i r_i^4}{r_i^3 - r_{i-1}^3} \quad (67)$$

$$-4p_i r_i + \frac{10p_{i+1} r_i^4}{-r_i^3 + r_{i+1}^3} + 4p_{i+1} r_i \quad (68)$$

$$c_i = \frac{M_i \rho_i}{2} - \frac{3M_i \rho_{i+1} r_{i+1}^3}{-2r_i^3 + 2r_{i+1}^3} + \frac{3M_i \rho_{i+1} r_{i+1}^2 r_{i-1}}{-2r_i^3 + 2r_{i+1}^3} + \frac{M_i \rho_{i+1}}{2} - \frac{10p_{i+1} r_i^2 r_{i+1}^2}{-r_i^3 + r_{i+1}^3} \quad (69)$$

$$d_i = \frac{M_i \rho_i r_{i+1}}{2} - \frac{M_i \rho_i r_{i-1}}{2} + \frac{M_i \rho_{i+1} r_{i+1}}{2} - \frac{M_i \rho_{i+1} r_{i-1}}{2} - 2p_i r_i^2 + 2p_{i+1} r_i^2 \quad (70)$$

The equation (65) is in fact a matrix equation. It could also be represented in the form:

$$\begin{pmatrix} b_1 & c_1 & & & 0 \\ a_2 & b_2 & c_2 & & \\ & a_3 & b_3 & \ddots & \\ & & \ddots & \ddots & c_{N-1} \\ 0 & & & a_N & b_N \end{pmatrix} \vec{\Delta r} = -\vec{d} \quad (71)$$

Equations of type of (71) are called tridiagonal matrix equations and can be solved with standard linear algebra methods. Especially the Tridiagonal matrix algorithm (TDMA) (also known as Thomas algorithm) [32], which we implemented, provides a fast way of computing the set of  $\Delta \tilde{r}_i$  that solves the hydrostatic equilibrium. Following the work of [17] we introduce boundary conditions and define a fixed innermost shell at coordinate origin ( $\tilde{r}_0 = 0$  and  $\Delta \tilde{r}_0 = 0$ ) and fix the position of the outermost shell ( $\Delta \tilde{r}_N = 0$ ). By doing so the number of equations reduces from  $N$  to  $N - 1$ . The latter condition has a technical and a physical dimension. The technical part is that the solving process of the tridiagonal matrix becomes very fast and efficient. The physical part which justifies this assumption is that the outer profile changes very little due to heat conduction in the inner region, so enforcing the boundary condition at  $\tilde{r}_N$  has little effect, if  $\tilde{r}_N$  is sufficiently large.

To reach the hydrostatic equilibrium several adjustment steps (iterations of the TDMA) are necessary. After each step the obtained  $\Delta\tilde{r}_i$  are used to adjust the thermodynamical properties  $\tilde{p}_i$  and  $\tilde{\rho}_i$  via (64) and (62). Now with those adjusted quantities the coefficients  $a$ ,  $b$ ,  $c$  and  $d$  can be computed and another adjustment step follows. This process ends when the system reaches the hydrostatic equilibrium, which we define as a sufficiently small relative change in radial adjustment  $\epsilon_r$ . We chose  $\epsilon_r = 10^{-3}$ , agreeing with [17]. In other words, the adjustment ends when

$$\max \left( \left| \frac{\Delta\tilde{r}_i}{\tilde{r}_i} \right| \right) < \epsilon_r \quad (72)$$

is fulfilled. Then the next heat conduction step is taken and the system is adjusted until equilibrium is reached again. In principal this evolution can be continued indefinitely, but "in practice, when core collapse occurs the densities rise sufficiently quickly that the [...] timestep becomes extremely small." [22].

## 5 Results

In this section, I will present the results of my research with the gravothermal fluid model. I will show that the model applies to self-interacting dark matter halos containing a central black hole. Furthermore, I will compare the obtained numerical profiles with semi-analytical predictions.

### 5.1 Adiabatic Black Hole Growth

The implementation of the gravothermal fluid model adiabatically adjusts the halo to maintain hydrostatic equilibrium while heat is conducted within the system. By introducing the central black hole in the system this process is altered. The additional gravitational pull changes the configuration of the equilibrium state. We have found that for mass ratios of

$$\frac{M_{BH}}{M_{DM}} \gtrsim 10^{-4}, \quad (73)$$

(where  $M_{BH}$  and  $M_{DM}$  denote the black hole mass and total dark matter mass respectively) it is not sufficient to just add the black hole mass in the hydrostatic equilibrium equation (36). If this is done the code fails to drive the system into an equilibrium state. Since these mass ratios apply to many galaxies like Milky Way-like galaxies and large galaxies like M87 (see [13] and [1]) they are of particular interest for probing the nature of dark matter through indirect observations. To make this range of the parameter space accessible for the gravothermal fluid model implementation it is necessary to improve the initial data frame. By starting from a small, slowly increasing black hole mass, we were able to continuously drive the system into hydrostatic equilibrium. In a way, the black hole is growing slowly such that the dark matter halo can adjust itself to the increasing gravitational pull. What is meant by adiabatic black hole growth is the quasi-static behavior of the system, continuously adjusting to the slowly increasing mass. For this work, we applied this loose definition and did not consider changes in entropy, etc. Once the black hole has reached its proper mass, the growth is stopped and time evolution begins (see Fig. 9).

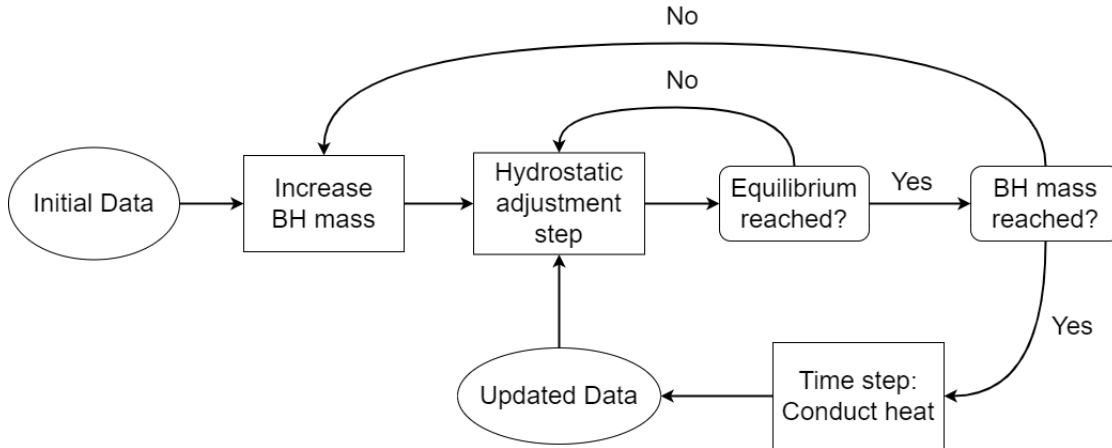


Figure 9: Flowchart of improved implementation: To simulate the adiabatic growth of the black hole, its mass is slowly increased while continuously adjusting the system to hydrostatic equilibrium. The growth process is stopped once the desired mass is reached. Then time evolution and heat conduction commences.

Though this may seem like an intrinsic shortcoming of the code, it is an important condition for the growth of a central dark matter density spike. In other words, only through the growing process of the black hole, it is possible to over-concentrate dark matter in the inner regions of the halo with the gravothermal fluid model. This agrees with the assumption taken in the semi-analytical approach to the problem in [9].

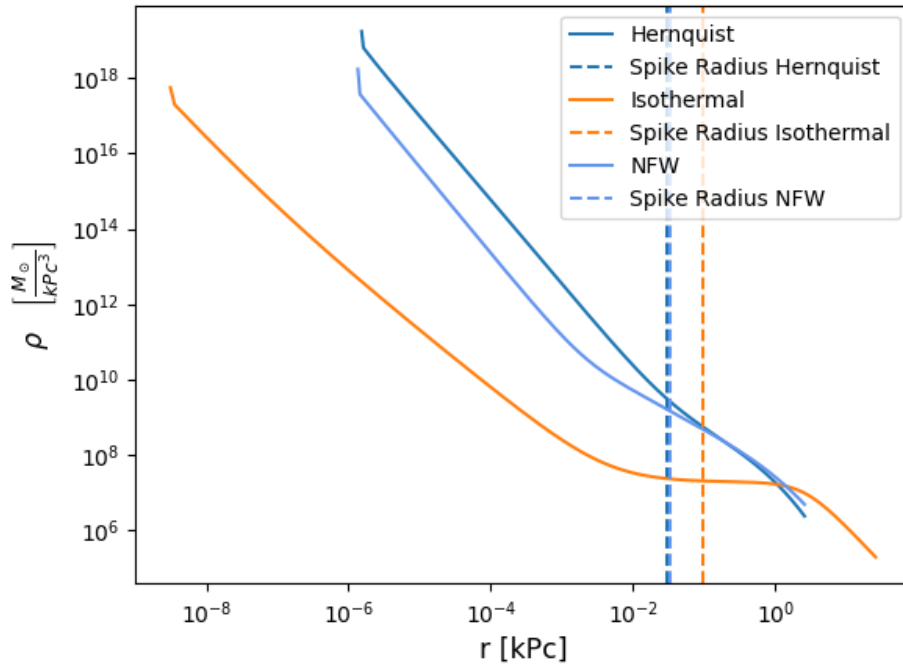
## 5.2 Initial Dark Matter Density Spike

With the presented implementation of the gravothermal fluid model extended by a central black hole, I was able to produce spiked density profiles. After the adiabatic growth of the black hole, the system reaches an equilibrium state and shows a significant increase in density for the inner regions. From the semi-analytical method of Gondolo and Silk (see Section 2.3), we have the predictions of the spike slope emerging from initial NFW, Hernquist and Isothermal profiles. In Fig. 10, the spiked density profiles and their slopes in log-log space are presented.

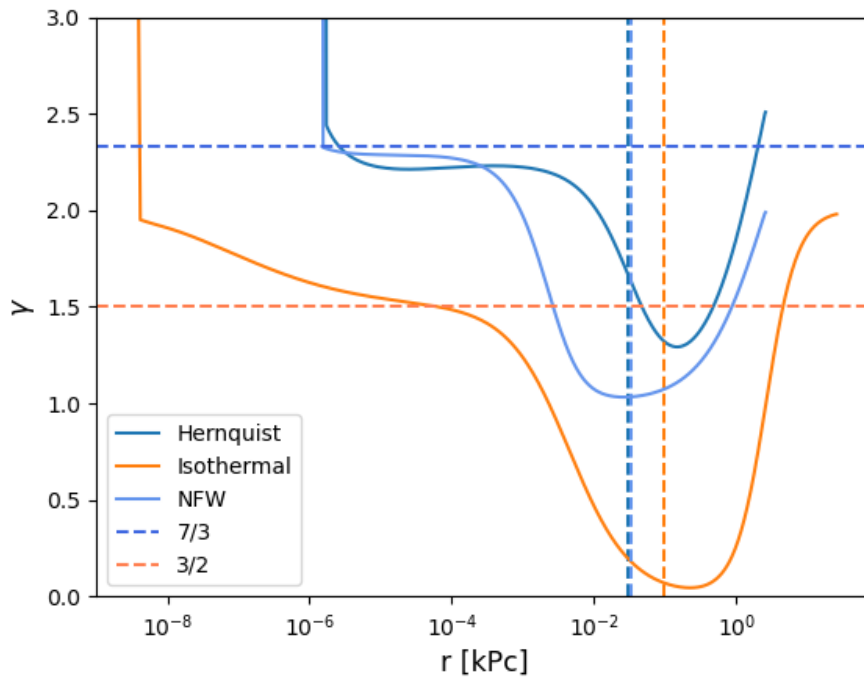
In plot 10(a) we can observe an approximately constant slope within the spike region for all three profiles and a gradual change to the original profiles in the outer regions (i.e. outside of the spike radius). Each profile carries a numerical artifact on the innermost point of the computation. This artifact is of particular interest and will be discussed in the section 6.2. In plot 10(b) inside the spike region, the NFW and Hernquist profiles have a slope of approximately  $\gamma_{sp} = 7/3$  agreeing with the prediction. The spike for the Isothermal profiles has a slope of approximately  $\gamma_{sp} = 3/2$  also agreeing with the prediction, but fits worse. For all profiles, we see the imprint of the numerical artifact in the slopes and a typical transition behavior around the spike radius.

With the presented implementation of the gravothermal fluid model, I was able to reproduce the semi-analytical predictions numerically!

When comparing the position of the spike obtained through the simulation with the spike radius, we find that the simulated spike lies within the spike region and is therefore expected to be physical!



(a) Spiked Density Profiles



(b) Slopes of the Spiked Density Profiles

Figure 10: 10(a) shows the numerically generated Isothermal, Hernquist and NFW profile for the inner regions of the halo. The vertical lines represent the corresponding spike radius  $r_{sp}$  for each profile. In 10(b) the slopes of the profiles are presented. Again the vertical lines correspond to the spike radius of each model and the horizontal lines to the semi-analytical predictions.

## 6 Conclusions

In this section, I am going to summarize the presented work and the key results. I will also discuss how the results can be used for future research and provide an outlook on how the model and the numerical simulation could be improved in the future.

### 6.1 Summary

In this thesis, I laid out the fundamental properties and the problems of the cold dark matter model. I introduced self-interacting dark matter as a possible solution to those unresolved phenomena and explained how dark matter structures (spherical dark matter halos) can be simulated with the gravothermal fluid model. This included explaining the method of Lagrangian Zones combined with the numerical process of continuously evolving the system. Previous research has shown that dark matter over-densities (dark matter spikes) in the center of dark matter halos are a powerful tool to examine the properties of dark matter (e.g. with gravitational waves). Those properties are crucial to prove the nature of dark matter and check whether self-interacting dark matter is an appropriate model. Dark matter spikes typically form around supermassive objects. So the goal of this work was to extend the gravothermal fluid model by adding a central black hole and study its impact on the density profile.

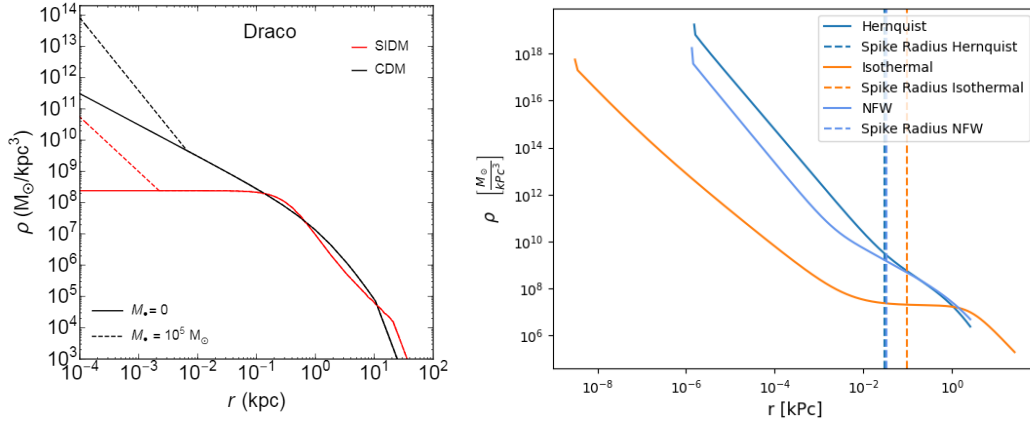
The two key results of this thesis are the following:

The implementation of the central black hole depends on the mass ratio between the black hole and the total dark matter mass. Above a typical ratio of  $\approx 10^{-4}$ , which applies to many galaxies, it is necessary to simulate the growth process of the central black hole and its feedback on the halo.

The presented implementation of the gravothermal fluid model with the central black hole is capable of producing realistic dark matter density spikes. In particular, the numerical simulation is now able to reproduce density spike slopes, which were semi-analytically predicted. The success here is that I was able to extend the gravothermal fluid model, in a way to produce realistic and

physical small scale phenomena.

This indicates that the numerical code we developed is capable of generating realistic systems through the gravothermal fluid model. This enables researchers to produce realistic and smooth dark matter distributions and use them for the analysis of spiked self-interacting dark matter halos. Before the common way was to artificially add a spike on top of a known density profile (see e.g. [1] and Fig. 11). With the extended model, it is now possible to simulate the inner and outer regions of the halo simultaneously and study the system as a whole.



(a) Artificially Spiked Density Profiles

(b) Numerical Spiked Density Profiles

Figure 11: Comparison of Spiked Density Profiles: Since [9] was published, spiked density profiles were generated like in 11(a). This means that one adds the semi-analytical prediction for the spike on top of a known profile at the spike radius. With the extended gravothermal fluid model, we can avoid this extension by hand and generate the correct and smooth profile directly from the fluid model like in 11(b). (Fig. 11(a) reprinted from [1])

## 6.2 Outlook

In my eyes, the gravothermal fluid model has a huge potential and offers many ways to advance it. The goal of this thesis was to extend the model and do the

groundwork for further research. In general, this further research can be split into two parts: extending the theoretical physical model and on the other hand improving the stability and capabilities of the implementation.

In terms of physics, one of the next steps could be to add more features of the central black hole to the model. Since we are already simulating the growth of the black hole, it is interesting to introduce mass accretion to the model. When doing so, one has to model a very violent environment, and the Newtonian treatment we applied needs to be extended by relativistic corrections. These corrections are already partially studied in [30]. Of course, a further generalization of the model is desirable. There are many ways to achieve that, e.g. the input density profile could be changed to a more generic one as studied in [9]. Also, the input properties of the self-interacting dark matter could be broadened. In this work, we assumed an elastic scattering with a constant cross-section, which is a plain assumption. By introducing inelastic scattering models as studied in [7] or velocity-dependent cross-sections as studied in [20] the spectrum of examinable self-interacting dark matter models is widened. Finally, the produced density profiles of this code can be used to study how the dark matter density spike affects the inspiral of massive objects and the so emitted gravitational waves.

Another point to improve is the implementation itself. While the interesting physics happens in heat conduction and time-evolution, the computationally most expensive process is maintaining the hydrostatic equilibrium. This solving of a tridiagonal matrix equation is one of the key processes that need to be done. The algorithm we implemented works well but is only semi-stable since it relies on the dominance of the main diagonal. This criterion is only fulfilled during the initial growth process. Once the heat is conducted, it fails and the algorithm breaks down, which is visually perceivable in the small numerical artifact in every density profile (see e.g. Fig. 11). If one succeeds to solve the issue and remove it, the stability could be restored. By improving this we could widen the parameter range in which the implementation is applicable. The algorithm could also be replaced by a parallel computing ansatz using GPUs, which would avoid the stability criterion and possibly works even faster.

## Literature

## References

- [1] Gerardo Alvarez and Hai-Bo Yu. “Density spikes near black holes in self-interacting dark matter halos and indirect detection constraints”. In: *Physical Review D* 104.4 (Aug. 2021). DOI: 10.1103/physrevd.104.043013. URL: <https://doi.org/10.1103%2Fphysrevd.104.043013>.
- [2] Shmuel Balberg, Stuart L. Shapiro, and Shogo Inagaki. “Self-Interacting Dark Matter Halos and the Gravo-thermal Catastrophe”. In: *The Astrophysical Journal* 568.2 (Apr. 2002), pp. 475–487. DOI: 10.1086/339038. URL: <https://doi.org/10.1086%2F339038>.
- [3] D. Baumann. *Cosmology*. Cambridge University Press, 2022. ISBN: 9781108838078. URL: <https://books.google.de/books?id=fAK1zgEACAAJ>.
- [4] Niklas Becker et al. “Circularization versus eccentrication in intermediate mass ratio inspirals inside dark matter spikes”. In: *Physical Review D* 105.6 (Mar. 2022). DOI: 10.1103/physrevd.105.063029. URL: <https://doi.org/10.1103%2Fphysrevd.105.063029>.
- [5] Edward Brown. “Stellar Astrophysics”. In: *Open Astrophysics Bookshelf* 39 (1 2017).
- [6] Kazunari Eda et al. “Gravitational waves as a probe of dark matter minispikes”. In: *Physical Review D* 91.4 (Feb. 2015). DOI: 10.1103/physrevd.91.044045. URL: <https://doi.org/10.1103%2Fphysrevd.91.044045>.
- [7] Rouven Essig et al. “Constraining Dissipative Dark Matter Self-Interactions”. In: (Sept. 2018). DOI: 10.1103/PhysRevLett.123.121102. URL: <http://arxiv.org/abs/1809.01144> <http://dx.doi.org/10.1103/PhysRevLett.123.121102>.
- [8] Katherine Garrett and Gintaras Duda. “Dark Matter: A Primer”. In: *Advances in Astronomy* 2011 (2011), pp. 1–22. DOI: 10.1155/2011/968283. URL: <https://doi.org/10.1155%2F2011%2F968283>.

- [9] Paolo Gondolo and Joseph Silk. “Dark Matter Annihilation at the Galactic Center”. In: *Physical Review Letters* 83.9 (Aug. 1999), pp. 1719–1722. DOI: 10.1103/physrevlett.83.1719. URL: <https://doi.org/10.1103/2Fphysrevlett.83.1719>.
- [10] Particle Data Group et al. “Review of Particle Physics”. In: *Progress of Theoretical and Experimental Physics* 2020.8 (Aug. 2020). 083C01. ISSN: 2050-3911. DOI: 10.1093/ptep/ptaa104. eprint: <https://academic.oup.com/ptep/article-pdf/2020/8/083C01/34673722/ptaa104.pdf>. URL: <https://doi.org/10.1093/ptep/ptaa104>.
- [11] James E. Gunn and III Gott J. Richard. “On the Infall of Matter Into Clusters of Galaxies and Some Effects on Their Evolution”. In: *The Astrophysical Journal* 176 (Aug. 1972), p. 1. DOI: 10.1086/151605.
- [12] Lars Hernquist. “An Analytical Model for Spherical Galaxies and Bulges”. In: *The Astrophysical Journal* 356 (June 1990), p. 359. DOI: 10.1086/168845.
- [13] Hai-Nan Lin and Xin Li. “The dark matter profiles in the Milky Way”. In: *Monthly Notices of the Royal Astronomical Society* 487.4 (June 2019), pp. 5679–5684. DOI: 10.1093/mnras/stz1698. URL: <https://doi.org/10.1093/2Fmnras%2Fstz1698>.
- [14] D. Lynden-Bell and P. P. Eggleton. “On the consequences of the gravothermal catastrophe”. In: *Monthly Notices of the Royal Astronomical Society* 191.3 (July 1980), pp. 483–498. ISSN: 0035-8711. DOI: 10.1093/mnras/191.3.483.
- [15] Stacy S. McGaugh, Michael K. Barker, and W. J. G. de Blok. “A Limit on the Cosmological Mass Density and Power Spectrum from the Rotation Curves of Low Surface Brightness Galaxies”. In: *The Astrophysical Journal* 584.2 (Feb. 2003), pp. 566–576. DOI: 10.1086/345806. URL: <https://doi.org/10.1086/2F345806>.
- [16] Julio F. Navarro, Carlos S. Frenk, and Simon D. M. White. “The Structure of Cold Dark Matter Halos”. In: *The Astrophysical Journal* 462 (May 1996), p. 563. DOI: 10.1086/177173. URL: <https://doi.org/10.1086/2F177173>.

- [17] Hiroya Nishikawa, Kimberly K. Boddy, and Manoj Kaplinghat. “Accelerated core collapse in tidally stripped self-interacting dark matter halos”. In: *Phys. Rev. D* 101 (6 Mar. 2020), p. 063009. DOI: 10.1103/PhysRevD.101.063009. URL: <https://link.aps.org/doi/10.1103/PhysRevD.101.063009>.
- [18] National Radio Astronomy Observatory. *The Mysterious Dark Energy*. URL: <https://public.nrao.edu/radio-astronomy/dark-energy/>.
- [19] Nobuhiro Okabe et al. “LoCuSS: The Mass Density Profile of Massive Galaxy Clusters at  $z=0.2$ ”. In: *The Astrophysical Journal* 769.2 (May 2013), p. L35. DOI: 10.1088/2041-8205/769/2/L35. URL: <https://doi.org/10.1088%2F2041-8205%2F769%2F2%2FL35>.
- [20] Nadav Joseph Outmeuguine et al. *Universal gravothermal evolution of isolated self-interacting dark matter halos for velocity-dependent cross sections*. 2022. DOI: 10.48550/ARXIV.2204.06568. URL: <https://arxiv.org/abs/2204.06568>.
- [21] P.J.E. Peebles. *Cosmology’s Century: An Inside History of Our Modern Understanding of the Universe*. Princeton University Press, 2022. ISBN: 9780691234472. URL: [https://books.google.de/books?id=%5C\\_tvKEAAAQBAJ](https://books.google.de/books?id=%5C_tvKEAAAQBAJ).
- [22] Jason Pollack. “Supermassive Black Holes from Gravothermal Collapse of Fractional Self-Interacting Dark Matter halos”. In: (May 2012). URL: [https://www.phas.ubc.ca/~jpollack/senior\\_thesis.pdf](https://www.phas.ubc.ca/~jpollack/senior_thesis.pdf).
- [23] A. Del Popolo. “The Cusp/Core problem and the Secondary Infall Model”. In: *The Astrophysical Journal* 698.2 (June 2009), pp. 2093–2113. DOI: 10.1088/0004-637x/698/2/2093. URL: <https://doi.org/10.1088%2F0004-637x%2F698%2F2%2F2093>.
- [24] Antonino Del Popolo and Morgan Le Delliou. “Small Scale Problems of the Lambda CDM Model: A Short Review”. In: *Galaxies* 5.1 (Feb. 2017), p. 17. DOI: 10.3390/galaxies5010017. URL: <https://doi.org/10.3390%2Fgalaxies5010017>.
- [25] James F Price. *Lagrangian and Eulerian Representations of Fluid Flow: Kinematics and the Equations of Motion*. 2006. URL: <https://www.who.edu/science/PO/people/jprice/class/ELreps.pdf>.

- [26] S. Price. Dec. 2015. URL: [https://mosdef.astro.berkeley.edu/wp-content/uploads/2015/12/rot\\_curve.png](https://mosdef.astro.berkeley.edu/wp-content/uploads/2015/12/rot_curve.png).
- [27] Andrew Robertson et al. “The surprising accuracy of isothermal Jeans modelling of self-interacting dark matter density profiles”. In: *Monthly Notices of the Royal Astronomical Society* 501.3 (Dec. 2020), pp. 4610–4634. DOI: 10.1093/mnras/staa3954. URL: <https://doi.org/10.1093%2Fmnras%2Fstaa3954>.
- [28] Matts Roos. “Dark Matter: The evidence from astronomy, astrophysics and cosmology”. In: (2010). DOI: 10.48550/ARXIV.1001.0316. URL: <https://arxiv.org/abs/1001.0316>.
- [29] Barbara Ryden. *Introduction to Cosmology*. 2nd ed. Cambridge University Press, 2016. DOI: 10.1017/9781316651087.
- [30] Stuart L. Shapiro. “Star clusters, self-interacting dark matter halos, and black hole cusps: The fluid conduction model and its extension to general relativity”. In: *Phys. Rev. D* 98 (2 July 2018), p. 023021. DOI: 10.1103/PhysRevD.98.023021. URL: <https://link.aps.org/doi/10.1103/PhysRevD.98.023021>.
- [31] Lyman Spitzer. *Dynamical evolution of globular clusters*. Princeton, New Jersey: Princeton University Press, 1987, 1 online resource (192 pages). ISBN: 9781400858736. URL: <http://www.jstor.org/stable/10.2307/j.ctt7ztvx4>.
- [32] L.H. Thomas. “Elliptic Problems in Linear Differential Equations over a Network”. In: *Watson Sci. Comput. Lab Report* (1949).
- [33] Sean Tulin and Hai-Bo Yu. “Dark matter self-interactions and small scale structure”. In: *Physics Reports* 730 (2018). Dark matter self-interactions and small scale structure, pp. 1–57. ISSN: 0370-1573. DOI: <https://doi.org/10.1016/j.physrep.2017.11.004>. URL: <https://www.sciencedirect.com/science/article/pii/S0370157317304039>.

## 7 Acknowledgement

This thesis was only made possible through a group of people who supported me over the last months. Many thanks go to my supervisor Laura Sagunski, who lead me to achieve this final step of my Bachelor's studies and the EXPLORE I group, especially to Charlotte, Niklas and Keiwan. Without their help this work would be less of a success. I also want to thank the whole DMGW group for the warm welcome and the useful discussions, which helped and motivated me in pursuing the project. Finally I want to thank my family for enabling me to fully focus on my studies.

## 8 Eigenständigkeitserklärung

Hiermit erkläre ich, dass ich die Arbeit selbstständig und ohne Benutzung anderer als der angegebenen Quellen und Hilfsmittel verfasst habe. Alle Stellen der Arbeit, die wörtlich oder sinngemäß aus Veröffentlichungen oder aus anderen fremden Texten entnommen wurden, sind von mir als solche kenntlich gemacht worden. Ferner erkläre ich, dass die Arbeit nicht - auch nicht auszugsweise - für eine andere Prüfung verwendet wurde.

Frankfurt am Main, den 19.05.2022

---